Vibrational Spectra of Nitrosyl-Substituted Transition-Metal Hydride Complexes: An Experimental and Theoretical Study of Carbonyldihydronitrosyl(trimethylphosphine)rhenium ($[Re(CO)H_2(NO)(PMe_3)_2]$)

by **Heiko Jacobsen**[a]), **Volker Jonas**[b])[1]), **David Werner**[b]), **Andreas Messmer**[a]), **Jan-Christoph Panitz**[c]), **Heinz Berke**[a])*, and **Walter Thiel**[b])*

[a]) Anorganisch-chemisches Institut, Universität Zürich-Irchel, Winterthurerstr. 190, CH-8057 Zürich
[b]) Organisch-chemisches Institut, Universität Zürich-Irchel, Winterthurerstr. 190, CH-8057 Zürich
[c]) Paul Scherrer Institut, CH-5232 Villigen PSI

The vibrational frequencies of carbonyldihydronitrosyl(trimethylphosphine)rhenium ($[Re(CO)H_2(NO)(PMe_3)_2]$; **1a**) and of its deuterated derivatives **1b** and **1c** have been investigated by IR and *Raman* spectroscopy (only **1a**) and by gradient-corrected density-functional calculations. Complex **1a** possesses two well separated $\tilde{\nu}_{ReH}$ stretching vibrational modes, which couple with the $\tilde{\nu}_{XO}$ stretching mode (X = N, C) of the ligand in *trans* position, but which do not couple with each other. These modes significantly differ in their IR intensities, so that only the $\tilde{\nu}_{ReH}$ band of the H-ligand *trans* to the nitrosyl ligand can be observed in the experiment. With *Raman* spectroscopy, both $\tilde{\nu}_{ReH}$ stretching vibrational modes can be observed. Computed frequencies, IR intensities, and force constants are presented. The influence of basis-set size and of the accuracy of the numerical integration scheme is investigated: the correct description of the intensities requires large basis sets and accurate numerical integration. Calculations have been extended to include the complexes $[Re(CO)H_2(NO)(PH_3)_2]$ (**2**) and $[Re(CO)H_2(NO)(PF_3)_2]$ (**3**) in order to study influences of different P-donor ligands.

1. Introduction. – One of the characteristic features of nitrosyl-substituted transition-metal-hydride complexes is their increased reactivity toward alkyne insertion and carbonyl reduction [1]. This effect is due to an enhanced 'hydridicity' of the H-ligand induced by the nitrosyl ligands. In the context of exploring the structural chemistry and reactivity of this class of compounds, we have synthesized a variety of dihydrorhenium complexes of the type $[Re(CO)H_2(NO)(PR_3)_2]$ (R = Me, Et, Cy, OMe, OEt, O^{i}Pr) [2]. We then performed protonation reactions to probe the hydridicity of these molecules [3]. During the course of our studies, we found that dihydrorhenium complexes are capable of undergoing a novel type of H-bonding interaction of the form MH···HX (M = metal), which is termed dihydrogen bonding [4]. In subsequent studies [5], we investigated the reaction of those complexes, which possess alkyl-substituted phosphine ligands, with acidic alcohols. Special emphasis was given to $[Re(CO)H_2(NO)(PMe_3)_2]$ (**1a**). Applying variable-temperature IR and NMR spectroscopy, T_{1min} measurements, and NOE experiments, we were able to characterize the nature of the dihydrogen bond, in terms of site preference as well as bond strengths.

---

[1]) Present address: *San Diego Supercomputer Center*, 9500 Gilman Drive, San Diego, CA 92093-0505, U.S.A.

Given this background, we decided to investigate the vibrational spectrum of $[Re(CO)H_2(NO)(PMe_3)_2]$ (**1a**) in more detail. In the present work, we mainly focus on the analysis of the $\tilde{\nu}_{NO}$, $\tilde{\nu}_{ReH}$, and $\tilde{\nu}_{CO}$ stretching frequencies of **1a**, since the changes in these modes under interaction with the acidic substrate contain valuable information about dihydrogen bonding. We want to identify the M-H stretching vibrations and determine the degree of coupling between these two modes, as well as between the $\tilde{\nu}_{XO}$ (X = C, N) and $\tilde{\nu}_{ReH}$ modes. To this end, we recorded IR and *Raman* spectra of **1a** in solution as well as in the solid state. Furthermore, IR data for the deuterated compounds $[Re(CO)DH(NO)(PMe_3)_2]$ (**1b**) and $[Re(CO)D_2(NO)(PMe_3)_2]$ (**1c**) were collected.

The experimental investigation is complemented by a computational study based on density-functional theory, which we have previously applied to investigate the vibrational spectra of transition-metal complexes [6], and in particular transition-metal hydrides [7]. Use was made of two common quantum-chemical program packages, namely Gaussian94 [8], and ADF, version 2.3 [9]. The main differences in these computational approaches lie in the choice of the basis functions, the treatment of core electrons, and the integral-evaluation techniques. The calculations were done not only to support the experimental assignments, but also to validate the computational methodology for further studies. Calculations on the model compounds $[Re(CO)H_2(NO)(PH_3)_2]$ (**2**) and $[Re(CO)H_2(NO)(PF_3)_2]$ (**3**) were included, in order to study the influence of different P-donor ligands.

2. Experimental Part. – *General*. All manipulations were performed under dry N_2 by standard *Schlenk*-tube techniques. $[Re(CO)H_2(NO)(PMe_3)_2]$ (**1a**) and $[Re(CO)DH(NO)(PMe_3)_2]$ (**1b**) were synthesized as described [2] [5b].

Carbonyldi[(²H)hydro]nitrosyl(trimethylphosphine)rhenium ($[Re(CO)D_2(NO)(PMe_3)_2]$; **1c**). A suspension of 170 mg (0.36 mmol) of $[Re(CO)Cl_2(NO)(PMe_3)_2]$ and 100 mg (2.39 mmol) of $NaBD_4$ in 20 ml of EtOH was heated to reflux for 45 min, the solvent evaporated, and the residue extracted with hexane. The yellow soln. was filtered through *Celite*. Evaporation afforded spectroscopically pure **1c** (quant.). Yellow powder that could be recrystallized from hexane.

Spectra. IR spectra: *BioRad-FTS-15E* and *BioRad-FTS-45* instruments; hexane solns. and KBr pellets. *Raman* spectra: *Dilor-LabRam-I-Raman* microscope (*Instruments SA*) equipped with a macro sampling device; anh. pentane soln. (*Fluka*), and as-prepared polycrystalline material, which was placed in a *Schlenk* tube. A He-Ne laser ($\lambda = 632.8$ nm) was used for the excitation of the spectra. To avoid sample decomposition, laser power at the polycrystalline sample was limited to less than 0.8 mW. For the solution spectra, a laser power of 7 mW at the sample was used. Data were recorded with a spectral resolution of 2.4 cm^{-1}. The calibration of band positions was performed by recording the spectra of Ne lamp (*Pen-Ray*, *Oriel*). Band positions and line widths were calculated using the 'peak-fitting module' implemented in the Origin™ program package (version 5.0, *Microcal Inc.* Northampton MA). *Voigt* functions with a fixed *Gaussian* contribution of 2.4 cm^{-1} were used in the nonlinear least-squares fit routines employed.

3. Computational Methods. – For $[Re(CO)H_2(NO)(PR_3)_2]$ (R = Me, H, F), gradient-corrected density-function calculations were carried out using the Gaussian94 [8] program system. Gradient corrections for exchange and for correlation were taken from the work of *Becke* [10] and *Perdew* [11], resp. (usually abbreviated as BP or BP86). Two basis sets were employed, labelled ECP1 and ECP2. Both use a quasi-relativistic effective core potential at the transition metal together with the corresponding (8s7p5d)/[6s5p3d] valence basis set [12] (for the BP86/ECP2 calculation, the original d splitting for Re was changed from (411) to (3111)). For all other atoms, ECP1 employs the 6-31G(d,p) basis [13], whereas ECP2 uses a (10s6p)/[5s3p]triple-ζ basis for C, N, and O [14], (5s)/[3s] for H [14] and (13s9p)/[6s5p] for P [15], supplemented by two sets of d polarization functions each [16]. Spherical d functions were applied throughout. Using analytic energy gradients, the molecular geometries were optimized within the constraint of C_s point-group symmetry. Second

derivatives were obtained by numerical differentiation of the analytic energy gradients. In the numerical integration of the functional and its derivatives, a *Lebedev* grid with 75 radial points and 302 angular points was used. The present computational approach is the same as in our previous studies [6] [7].

For $[Re(CO)H_2(NO)(PMe_3)_2]$ (**1a**) and $[Re(CO)H_2(NO)(PH_3)_2]$ (**2**), additional BP86 calculations were performed with the ADF program package, version 2.3 [9]. Again, two different basis sets were utilized, called FCA1 and FCA2. In both cases, use of the frozen-core approximation was made, and the *n*s, *n*p, *n*d, and $(n+1)$s shells of the transition metal were described by a triple ζ-STO basis augmented by one $(n+1)$p function (ADF database IV). For FCA1, the valence shells of the main-group atoms were described by a double ζ-STO basis plus one polarization function (ADF database III). FCA2 represents a triple ζ-STO basis augmented by two polarization functions (ADF database V). In the FCA2 calculation for **1a**, the Me groups of the phosphine ligands were treated with the ADF database III. The numerical integration was based on a method developed by *te Velde* [9b]. The grid was chosen such that an internal set of standard integrals was evaluated with an accuracy of five or six significant digits for geometry optimizations or frequency calculations, resp. Derivatives of the energy were calculated according to the same methods as mentioned above [17]. The calculations for $[Re(CO)H_2(NO)(PMe_3)_2]$ (**1a**) were performed in C_s symmetry, whereas for $[Re(CO)H_2(NO)(PH_3)_2]$ (**2**) no symmetry constraints were employed. Relativistic effects were included using a quasi-relativistic approach [18].

The program INTDER95[2]) was used to perform the transformation of force constants and dipole-moment derivatives from cartesian coordinates to internal coordinates.

4. Results and Discussion. – *Molecular Structures.* In *Fig. 1*, an exemplary geometry of **1a** is displayed, obtained from a BP86/FCA2 calculation. The ideal coordination polyhedron is distorted in a way that the two phosphine ligands are bent towards the H-ligands. This structural motif is characteristic for all calculated complexes, and can also be found in the solid-state structure [2] of $[Re(CO)H_2(NO)(P(OMe)_3)_2]$ (**4**). A brief inspection of selected optimized geometric parameters (*Table 1*) reveals that all calculations for a given molecule result in comparable molecular structures, in which the bond distances and bond angles typically differ by only 1–2 pm or 1–2 degree, respectively. An exception is the coordination geometry of the PR_3 ligand where larger variations in bond distances and angles are present. Furthermore, the geometry of the PH_3 complex **2** is similar to that of **1a** since the deviations are not larger than those found by variation of the basis set for **1a** or **2** (see *Table 1*). For the FCA2 calculation, the mean differences in the reported bond lengths and bond angles between **1a** and **2** amount to only 0.25 and 0.40%, respectively, if the angle P–Re–P is excluded.

The reported structural parameters [2] for $[Re(CO)H_2(NO)(P(OMe)_3)_2]$ (**4**), namely Re–C 196(1) pm, Re–N 178(1) pm, Re–P 237.5(5) and 234.2(5) pm, N–Re–C 102.5(6)°, and P–Re–P 160.0(2)° are in fair agreement with the calculated values for **2**, which resembles **4** closest in the combination of electronic and steric properties [19]. Although the bond distances seem to be overestimated in the calculation, which is most pronounced for the Re–N bond, the overall geometric arrangement is well reproduced.

Vibrational Frequencies. The experimental IR spectrum of **1a** in hexane solution, in the region between 1600 and 2000 cm^{-1}, shows three bands, belonging to the $\tilde{\nu}_{NO}$, $\tilde{\nu}_{CO}$ and $\tilde{\nu}_{ReH}$ stretches (*Table 2*). The first two are strong in intensity and fairly sharp, $\tilde{\nu}_{CO}$ representing the most intense band. The $\tilde{\nu}_{ReH}$ band is *ca.* 6–8 times weaker, compared to $\tilde{\nu}_{XO}$ (X = N, C), and of larger line-width. When the IR-spectrum of **1a** is recorded for a KBr pellet, a shift to lower wave numbers by 20–30 cm^{-1} is observed for the $\tilde{\nu}_{XO}$

---

[2]) INTDER95 is a general program developed by *Wesley D. Allen* and co-workers which performs various vibrational analyses and higher-order nonlinear transformations among force-field representations.

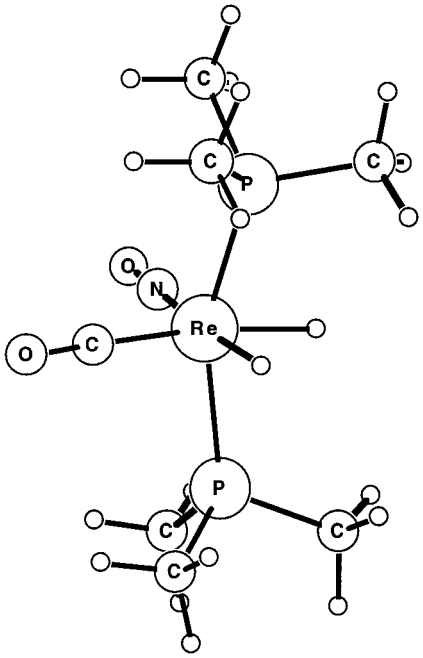

Fig. 1. *The molecular structure of [Re(CO)H$_2$(NO)(PMe$_3$)$_2$]* **1a**, *obtained from a BP86/FCA2 geometry optimization*

Table 1. *Selected Geometric Parameters* [a]) *for [Re(CO)H$_2$(NO)(PR$_3$)$_2$],* (R = Me, H, F) *Obtained from Geometry Optimizations Employing Different Basis Sets*

	1a, (R = Me)			**2** (R = H)				**3** (R = F)
	ECP1	FCA1	FCA2	ECP1	ECP2	FCA1	FCA2	ECP1
Re–H$^{t\text{-}NO}$ [b])	175.8	174.6	174.1	175.0	175.3	174.1	174.4	174.3
Re–H$^{t\text{-}CO}$ [b])	173.4	171.8	170.9	172.9	173.0	171.6	171.0	172.3
Re–N	183.9	183.5	182.7	184.5	184.2	183.6	183.6	185.6
Re–C	198.0	197.1	197.5	199.0	199.2	198.5	199.0	201.3
Re–P	241.4	240.2	237.0	238.9	239.2	[c])	237.0	231.5
N–O	119.8	119.6	118.9	119.1	118.2	119.0	118.3	117.9
C–O	117.8	117.2	116.3	117.3	116.2	116.5	116.1	116.4
H–Re–H	78.6	74.2	76.9	77.3	77.7	77.1	77.3	79.1
N–Re–C	102.4	107.8	103.5	103.6	103.2	104.3	103.9	102.9
P–Re–P	154.0	161.5	152.8	154.3	153.9	155.4	158.6	150.3

[a]) In pm and degree. [b]) H$^{t\text{-}NO}$ denotes the H-ligand in *trans* position to NO, whereas H$^{t\text{-}CO}$ stands for the H ligand *trans* to CO; *cf.* also *Fig. 1*. [c]) The FCA1 calculation without symmetry constraints yielded slightly different Re–P bond lengths of 239.0 and 238.3 pm.

stretches, whereas $\tilde{\nu}_{ReH}$ does not show a substantial shift. Furthermore, additional bands are observed in the $\tilde{\nu}_{ReH}$ region. The question whether one of those represents a second Re–H stretching mode, could be answered by means of *Raman* spectroscopy. The band positions of the *Raman* spectra of **1a** in pentane solution are in very good agreement

with the IR results, and differ by *ca.* 1 cm^{-1} (*Table 3*). In the $\tilde{\nu}_{ReH}$ region, we now observe two bands of different intensity, separated by 31 cm^{-1}, of which the one at lower wave numbers corresponds to the absorption found in the IR experiment. In the *Raman* spectrum of **1a** in the solid state, we see two additional, and a total of four bands in the $\tilde{\nu}_{ReH}$ region. Three bands are discernible from the raw spectrum, and the fourth band is located on the high-wave-number shoulder of the band profile. Band positions listed in *Table 3* are the results of the nonlinear least-squares calculations performed. Two of these signals correspond in band position to the modes observed in solution, and should be assigned as Re–H stretching modes. The other two are similar in band position to the additional bands observed in the IR, and are probably due to a symmetry induced splitting caused by packing the molecules in the unit cell of the crystal.

We conclude from these experiments that $[Re(CO)H_2(NO)(PMe_3)_2]$ (**1a**) has two different Re–H stretching modes, well separated in energy by *ca.* 30 cm^{-1}. Compared to $\tilde{\nu}_{NO}$ and $\tilde{\nu}_{CO}$, the relative IR intensities have to be classified as weak and very weak, so that only one of them can be observed in the IR spectrum.

Table 2. *Experimental IR Spectra* [a]) *for* $[Re(CO)H_2(NO)(PMe_3)_2]$ (**1a**) *and its Deuterated Derivatives* **1b** *and* **1c** *in the Region of* $\tilde{\nu}_{NO}$, $\tilde{\nu}_{ReH}$, *and* $\tilde{\nu}_{CO}$. Relative intensities [b]) are given in parentheses.

		1a	**1b**	**1c**
Hexane solution	$\tilde{\nu}_{NO}$	1657 (0.87)	1659 (0.49)	–
		–	1679 (0.68)	1680 (0.82)
	$\tilde{\nu}_{ReH}$	1799 (0.14)	1799 (0.10)	
	$\tilde{\nu}_{CO}$	–	1961 (1.00)	1960 (1.00)
		1967 (1.00)	1965 (0.91)	–
KBr pellet	$\tilde{\nu}_{NO}$	1630 (0.87)	1636 (0.82)	[c])
		–	1653 (0.83)	[c])
	$\tilde{\nu}_{ReH}$	1788 (0.52)	1788 (0.42)	[c])
		1802 (0.45)	1803 (0.37)	[c])
		1821 [d])	–	[c])
	$\tilde{\nu}_{CO}$	–	1938 (1.00)	[c])
		1944 [e]) (1.00)	1945 [d])	[c])

[a]) In cm^{-1}. [b]) Obtained from values for maximum height. [c]) Not measured. [d]) Shoulder. [e]) Additional shoulder at 1905 cm^{-1}.

Table 3. *Experimental* Raman *Spectra* [a]) *of* $[Re(CO)H_2(NO)(PMe_3)_2]$ (**1a**) *in the Region of* $\tilde{\nu}_{NO}$, $\tilde{\nu}_{ReH}$, *and* $\tilde{\nu}_{CO}$. Relative intensities [b]) are given in parentheses.

	Pentane solution	Solid state
$\tilde{\nu}_{NO}$	–	1632
	1656 (1.00)	1654
$\tilde{\nu}_{ReH}$	–	1790
	1800 (0.10)	1803
	–	1823
	1831 (0.30)	1830
$\tilde{\nu}_{CO}$	1967 (0.34)	1945

[a]) In cm^{-1}. [b]) Obtained from values for maximum height.

Calculated IR spectra of **1a**, **2**, and **3** are presented in *Table 4*. For **1a**, both the ECP and FCA methods overestimate the value for $\tilde{\nu}_{NO}$, the latter being somewhat closer to the experiment. One should, however, keep in mind that our comparison is made between calculated values for an isolated molecule and measured solution spectra. Values for the CO stretching frequencies of transition-metal carbonyl hydrides measured in gas phase and in solution typically differ by *ca.* 10 cm^{-1}, where $\tilde{\nu}_{CO}$ in solution normally appears at lower wave numbers (*cf.* [7] and lit. cit. therein). Similar effects can be expected for transition-metal nitrosyl hydrides. In the ECP approach, the value of $\tilde{\nu}_{CO}$ is already well reproduced with a medium-size basis set, while the FCA calculation requires a large basis to obtain results of similar quality. Both calculations utilizing the medium-size basis set show for the Re–H stretching modes a separation of *ca.* 10 cm^{-1}, whereas an increase of the basis from FCA1 to FCA2 raises this splitting to 24 cm^{-1}, in good agreement with the experimental result. In general, the calculated values for $\tilde{\nu}_{ReH}$ also seem to be overestimated.

Table 4. *Calculated IR Spectra* [a]) *for [Re(CO)H$_2$(NO)(PR$_3$)$_2$], (R = Me, H, F) in the Region of $\tilde{\nu}_{NO}$, $\tilde{\nu}_{ReH}$, and $\tilde{\nu}_{CO}$*

	1a (R = Me)			**2** (R = H)				**3** (R = F)
	ECP1	FCA1	FCA2	ECP1	ECP2	FCA1	FCA2	ECP1
$\tilde{\nu}_{NO}$	1714	1680	1689	1747	1712	1709	1708	1798
$\tilde{\nu}_{ReH}$	1831	1851	1839	1859	1850	1879	1838	1902
	1842	1858	1863	1864	1862	1888	1865	1907
$\tilde{\nu}_{CO}$	1960	1937	1963	1987	1976	1969	1981	2037

[a]) In cm^{-1}.

For complex **2**, basis-set effects have been studied both for the ECP and the FCA approach. There are no uniform trends, even though the computed vibrational frequencies tend to decrease slightly, by *ca.* 1%, upon basis-set enlargement (ECP1 → ECP2, FCA1 → FCA2). We will return to the IR spectra of **2** and **3** at a later point in our discussion.

Infrared Intensities. Among all the calculated IR intensities for **1a**, **2**, and **3**, the CO stretch represents the most intense mode, normally followed by the NO stretch (*Table 5*). For **1a**, this matches the experimental findings. Considering the intensities of the two $\tilde{\nu}_{ReH}$ modes in **1a**, ECP1 yields values that differ by a factor of 10, the low-frequency mode being the intense one. While this is consistent with the measured IR spectrum (hexane) which shows only one $\tilde{\nu}_{ReH}$ band, the prediction that $\tilde{\nu}_{ReH}$ is stronger than $\tilde{\nu}_{NO}$ is not in accord with the experimental result. FCA1 produces two similar Re–H intensities for **1a** which are *ca.* 5 times weaker than $\tilde{\nu}_{CO}$. Increasing the basis set improves the description. For FCA2, only one $\tilde{\nu}_{ReH}$ possesses significant intensity, and the relative order $I(\tilde{\nu}_{CO}) > I(\tilde{\nu}_{NO}) > I(\tilde{\nu}_{ReH})$ matches the experimentally observed trend, although the value for $I(\tilde{\nu}_{ReH})$ appears to be too high.

For **2**, the computed IR intensities for $\tilde{\nu}_{NO}$ and $\tilde{\nu}_{CO}$ are not overly basis-set dependent, while there is a dramatic sensitivity for $\tilde{\nu}_{ReH}$: The higher-frequency $\tilde{\nu}_{ReH}$ mode is slightly more intense than its lower-frequency counterpart for medium-sized basis sets (ECP1, FCA1), but less intense, by factors of *ca.* 6 or 50, for the larger basis sets (ECP2, FCA2). Related to this problem, we also investigated dependencies on the

Table 5. *$\tilde{\nu}_{NO}$, $\tilde{\nu}_{ReH}$, and $\tilde{\nu}_{CO}$ IR Intensities* [a]) *for [Re(CO)H$_2$(NO)(PR$_3$)$_2$]* (R = Me, H, F)

	1a (R = Me)			**2** (R = H)				**3** (R = F)
	ECP1	FCA1	FCA2	ECP1	ECP2	FCA1	FCA2	ECP1
$\tilde{\nu}_{NO}$	363	616	550	430	593	688	560	440
$\tilde{\nu}_{ReH}$	403	147	415	112	346	126	463	148
	42	152	16	331	55	192	9	243
$\tilde{\nu}_{CO}$	701	707	796	723	800	786	822	617

[a]) In km/mol.

accuracy of the numerical integration scheme. To this end, test calculations were performed for **2**, using the medium-size basis sets but a larger number of points in the numerical integration. Whereas the geometry and frequencies virtually do not change when the numerical accuracy is increased, a sizeable effect is found for the computed intensities, which again demonstrates their sensitivity to the chosen computational approach.

The question remains whether these changes in the theoretical IR intensities are caused by changes in the cartesian dipole-moment derivatives or in the composition of the normal modes. We, therefore, performed calculations for **1a** in which the FCA2 intensities were calculated using the FCA1 dipole-moment derivatives, FCA2$_{FCA1}$, and *vice versa*. Although the values for $I(\tilde{\nu}_{ReH})$ do change (FCA2$_{FCA1}$: 315, 33 km/mol; FCA1$_{FCA2}$: 207, 136 km/mol), the qualitative picture, namely two $I(\tilde{\nu}_{ReH})$ values of comparable magnitude for FCA1 and two very different $I(\tilde{\nu}_{ReH})$ values for FCA2, remains the same. This implies that the changes in the contribution of different internal coordinates to one particular vibration, and not the changes in the dipole-moment derivatives, are mainly responsible for the alteration in the IR intensities under basis-set extension. In the next section, we address this problem in more detail, in connection with an assignment of what we call the Re–H stretching modes.

Vibrational Assignment of the Re–H Stretches. The analysis of vibrational spectra is best done in chemically meaningful internal coordinates so that the cartesian force constants, resulting from the quantum-chemical calculations, need to be transformed. The four bond stretches representing the most important internal coordinates are s_1 = C–O, s_2 = N–O, s_3 = Re–H$^{t\text{-}NO}$, s_4 = Re–H$^{t\text{-}CO}$[3]). Values for quadratic force constants in internal coordinates can be found in *Table 6*. The off-diagonal elements of the force-constant matrix *F* may look negligible compared to the diagonal ones, but they will determine the more subtle details of the spectra. The size of the matrix elements is comparable to that of experimentally determined force constants. As an example, we mention the complex [Os(CO)H$_2$(mes)] (mes = 2,4,6-Me$_3$C$_6$H$_3$). The normal-coordinate analysis for this molecule was performed by *Polzer* and *Kiefer* [20] based on the results of IR and *Raman* measurements. They found, *e.g.*[4]), F_{11} = 13.314, F_{33} = 2.517, F_{13} = 0.036, and F_{23} = 0.002 (in N/cm).

---

[3]) H$^{t\text{-}NO}$ = H-ligand *trans* to NO, H$^{t\text{-}CO}$ = H-ligand *trans* to CO; the same holds for D-ligands.

[4]) The internal coordinates were defined as described above, with Re replaced by Os.

Table 6. *Quadratic Force Constants* [a]) *in Internal Coordinates* [b]) *for [Re(CO)H$_2$(NO)(PR$_3$)$_2$]* (R = Me, H, F)

	1a (R = Me)			**2** (R = H)				**3** (R = F)
	ECP1	FCA1	FCA2	ECP1	ECP2	FCA1	FCA2	ECP1
F_{11}	15.074	14.620	15.095	15.575	15.406	15.175	15.494	16.440
F_{22}	12.562	11.753	12.042	13.115	12.489	12.233	12.497	14.036
F_{33}	1.923	1.992	1.950	1.989	1.975	2.057	1.938	2.078
F_{44}	2.016	2.071	2.081	2.061	2.065	2.133	2.077	2.157
F_{12}	0.182	0.193	0.210	0.176	0.198	0.205	0.216	0.165
F_{13}	0.039	0.033	0.043	0.033	0.035	0.034	0.034	0.020
F_{14}	−0.001	−0.005	−0.001	−0.005	−0.007	−0.003	−0.004	−0.008
F_{23}	−0.005	−0.003	0.001	−0.012	−0.008	−0.005	−0.005	−0.020
F_{24}	0.052	0.060	0.061	0.048	0.053	0.049	0.056	0.034
F_{34}	0.021	0.008	0.008	0.015	0.013	0.010	0.008	0.016

[a]) In N/cm. [b]) See text for the definition of the internal coordinates.

All calculations show that the force constant F_{33} belonging to the Re–H$^{t\text{-NO}}$ stretch[3]) is lower than that of the Re–H$^{t\text{-CO}}$ stretch (F_{44}). This is indicative for a somewhat weaker or more activated Re–H$^{t\text{-NO}}$ bond. In general, the interaction force constants are not very sensitive to changes in the basis set. Concerning the coupling between the Re–H and X–O stretches, it is somewhat surprising that the *cis* interactions (F_{13}, F_{24}) are larger in absolute value than the *trans* interactions (F_{14}, F_{23}). On the other hand, the coupling force constant F_{34} between the two Re–H stretches is quite small, as expected.

A clearer picture can be obtained when the vibrational modes are characterized by the dominant components in the potential-energy distribution. Such an analysis is provided in *Table 7*. Thus, in calculations employing a medium-size basis set, the two Re–H stretching modes do significantly couple with each other. Increasing the basis set diminishes this coupling, and the contributions to the Re–H modes only stem from one particular Re–H stretch and the X–O stretch of the ligand in *trans* position.

We can now describe the coupling in which Re–H stretches are involved as follows. The unperturbed modes are assumed to be ordered in energy as $\tilde{\nu}_{NO} < \tilde{\nu}_{ReH}{}^{t\text{-NO}} < \tilde{\nu}_{ReH}{}^{t\text{-CO}} < \tilde{\nu}_{CO}$. When the first two modes couple, the in-phase combination will be

Table 7. *Vibrational Assignment for Re–H Stretching Frequencies* [a]) *for* **1a** *and* **2** *in Terms of Potential-Energy Distributions*

		Potential-energy distribution [b])
1a (R = Me)	FCA1	1851 cm^{-1}: $0.59 \cdot s_3 - 0.24\ s_4 - 0.08 \cdot s_2 - 0.07 \cdot s_1$ 1858 cm^{-1}: $0.53 \cdot s_4 + 0.30 \cdot s_3 + 0.15 \cdot s_1$
	FCA2	1839 cm^{-1}: $0.84 \cdot s_3 - 0.13 \cdot s_2$ 1863 cm^{-1}: $0.80 \cdot s_4 + 0.16 \cdot s_1$
2 (R = H)	FCA1	1879 cm^{-1}: $0.45 \cdot s_3 - 0.36 \cdot s_4 - 0.10 \cdot s_2 - 0.07 \cdot s_1$ 1888 cm^{-1}: $0.43 \cdot s_4 + 0.43 \cdot s_3 + 0.12 \cdot s_1$
	FCA2	1838 cm^{-1}: $0.79 \cdot s_3 - 0.18 \cdot s_2$ 1865 cm^{-1}: $0.87 \cdot s_4 + 0.11 \cdot s_1$

[a]) See text for the definition of the internal coordinates. [b]) Components below 5% are omitted.

dominated by $\tilde{\nu}_{NO}$ and will be lowered in energy. The main contributor to the out-of-phase combination will be the $\tilde{\nu}_{ReH}{}^{t\text{-}NO}$ mode. In the out-of-phase coupling, the two stretching modes enhance each other so that $\tilde{\nu}_{ReH}{}^{t\text{-}NO}$ will gain intensity, and $\tilde{\nu}_{NO}$ will become weaker. For the other two modes, $\tilde{\nu}_{ReH}{}^{t\text{-}CO}$ and $\tilde{\nu}_{CO}$, the opposite holds. Coupling will lower the energy as well as the intensity of $\tilde{\nu}_{ReH}{}^{t\text{-}CO}$. The $\tilde{\nu}_{CO}$ mode will be shifted to higher wave numbers and increase in intensity. The coupling of the Re–H stretches only with the X–O stretch of the ligand in *trans* position, therefore, results in two $\tilde{\nu}_{ReH}$ modes of different intensities. Furthermore, the coupling should decrease the inherent energy difference of the two $\tilde{\nu}_{ReH}$ modes. We have checked the coupling scheme as presented here in deuteration experiments that allow for a decoupling of the $\tilde{\nu}_{ReH}$ and the respective $\tilde{\nu}_{XO}$ modes.

Effect of Deuteration. The IR spectrum for the monodeuterated compound [Re(CO)DH(NO)(PMe_3)$_2$] (**1b**) is displayed in *Fig. 2*, and the corresponding band positions are also compiled in *Table 2*. Complex **1b** is a mixture of the two isomers [Re(CO)($D^{t\text{-}NO}$)H(NO)(PMe_3)$_2$] (**1b**$^{t\text{-}NO}$) and [Re(CO)($D^{t\text{-}CO}$)H(NO)(PMe_3)$_2$] (**1b**$^{t\text{-}CO}$)[3]). Two bands are found in the N–O stretching region, one at 1659 cm^{-1}, close to $\tilde{\nu}_{NO}$ of **1a** and thus assigned to **1b**$^{t\text{-}NO}$, and one new band at 1679 cm^{-1}, which essentially represents an uncoupled[5]) $\tilde{\nu}_{NO}$ mode in **1b**$^{t\text{-}CO}$. The latter band is more intense, as predicted by our coupling scheme. The $\tilde{\nu}_{ReH}$ band at 1799 cm^{-1} remains unshifted compared to that of **1a**. This confirms that the Re–H stretches indeed are not coupled. In the $\tilde{\nu}_{CO}$ region, a second band appears shifted to lower wave numbers by 4 cm^{-1}. Unexpectedly, the new band representing uncoupled $\tilde{\nu}_{CO}$ is the strongest one. One has to keep in mind, however, that the two species **1b**$^{t\text{-}CO}$ and **1b**$^{t\text{-}NO}$ might have different concentrations in the measured sample. It is thus possible that $\tilde{\nu}_{CO}$ uncoupled is more intense than $\tilde{\nu}_{CO}$ coupled because the formation of **1b**$^{t\text{-}CO}$ is favored over the formation of **1b**$^{t\text{-}NO}$.

The IR data of the fully deuterated complex [Re(CO)D_2(NO)(PMe_3)$_2$] (**1c**) (see *Table 2*) reveal that the positions of the $\tilde{\nu}_{NO}$ and $\tilde{\nu}_{CO}$ bands are practically identical to those observed for **1b**. This again points to the fact that the $\tilde{\nu}_{XO}$ stretches only couple with one of the two $\tilde{\nu}_{ReH}$ modes, *i.e.*, the one in *trans*-position.

Both ECP as well as FCA calculations of the IR spectra for **1a**–**c** (see *Table 8*) support the coupling scheme as outlined above. The different modes shift in position and intensity as predicted. This also holds for $\tilde{\nu}_{CO}$, which does shift to lower wave numbers and loses intensity when decoupled from the $\tilde{\nu}_{ReH}$ stretch. In the fully deuterated compound **1c**, both $\tilde{\nu}_{ReD}$ stretches are of low intensity and are separated by 43 cm^{-1} (ECP1) or 46 cm^{-1} (FCA2). $\tilde{\nu}_{ReD}$ in *trans* position to the nitrosyl ligand appears at lower frequencies than $\tilde{\nu}_{ReD}$ *trans* to CO, consistent with a more activated Re–$D^{t\text{-}NO}$ or Re–$H^{t\text{-}NO}$ bond.

Influence of Different P-Donor Ligands. The last point we would like to address is how the electronic properties of the P-donor ligands are reflected in the IR spectra. Thus, frequencies for molecules of the type [Re(CO)H_2(NO)(PR_3)] with three different P-ligands, namely R = Me (see **1a**), H (see **2**), and F (see **3**), were calculated on the ECP1 level. A good σ-donor ligand will increase the electron density at the metal

---

[5]) Strictly speaking, ν_{NO} and ν_{CO} can couple not only with ν_{ReH}, but also with ν_{ReN} and ν_{ReC}. In the FCA2 calculation for ReD_2(NO)(CO)(PMe_3)$_2$ **1c**, these contributions in the PED are around 0.10.

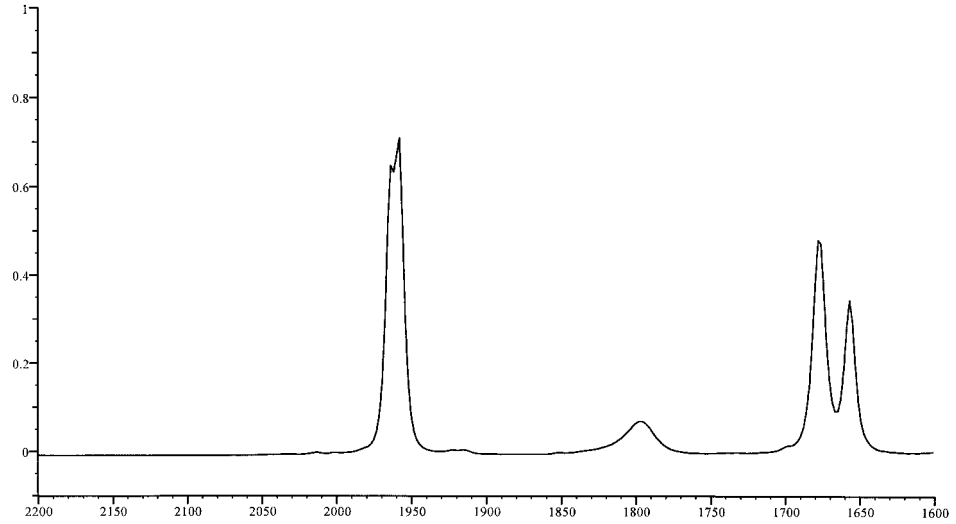

Fig. 2. *IR Spectrum of [Re(CO)DH(NO)(PMe$_3$)$_2$]* (**1b**), *recorded in hexane solution*

Table 8. *Calculated IR frequencies* [a]) *and intensities* [b]) (in parentheses) *for [Re(CO)Y$_2$(NO)(PMe$_3$)$_2$]*, (Y = H, D)

$Y^{t\text{-}NO}$	$Y^{t\text{-}CO}$	ECP1				FCA2			
		$\tilde{\nu}_{NO}$	$\tilde{\nu}_{ReY}{}^{t\text{-}NO}$	$\tilde{\nu}_{ReY}{}^{t\text{-}CO}$	$\tilde{\nu}_{CO}$	$\tilde{\nu}_{NO}$	$\tilde{\nu}_{ReY}{}^{t\text{-}NO}$	$\nu_{ReY}{}^{t\text{-}CO}$	$\tilde{\nu}_{CO}$
H	H	1714(363)	1831(403)	1842(42)	1960(701)	1689(550)	1839(416)	1863(16)	1963(796)
D	H	1747(747)	1271(49)	1842(4)	1960(700)	1716(898)	1286(8)	1863(4)	1963(796)
H	D	1717(362)	1831(435)	1313(25)	1950(625)	1691(544)	1839(423)	1330(42)	1948(704)
D	D	1749(740)	1271(37)	1314(32)	1950(623)	1718(889)	1285(4)	1331(51)	1948(702)

[a]) In cm^{-1}. [b]) In km/mol.

center, and thus the amount of backbonding to the π-accepting XO ligands. This in turn will lower $\tilde{\nu}_{XO}$, which then can be used as a relative measure for the σ-donor strength of the PR_3 ligand. On the other hand, the H-ligand also binds through σ donation to the metal center, and in this way competes with the P-ligand. Effective σ donation from the PR_3 ligand leads to a weakened Re–H bond, and to lower $\tilde{\nu}_{ReH}$ wave numbers. The position of $\tilde{\nu}_{ReH}$ also correlates with the σ-donor capacity of the PR_3 ligand. The calculations reveal the following trends (*cf. Table 4*): $\tilde{\nu}_{XO}$ (**1a**) $< \tilde{\nu}_{XO}$ (**2**) $< \tilde{\nu}_{XO}$ (**3**), and $\tilde{\nu}_{ReH}$ (**1a**) $< \tilde{\nu}_{ReH}$ (**2**) $< \tilde{\nu}_{ReH}$ (**3**). Both of these observations lead to the expected ranking in σ-donor strength: $PMe_3 > PH_3 > PF_3$. The changes in the spectra after substitution on the P-ligand are significant, *e.g.* shifts of 30 cm^{-1} and higher. This limits the use of PH_3 as a simple model ligand for computationally more demanding phosphines in frequency calculations.

5. Conclusion. – The main results of the present study are: [Re(CO)H_2-(NO)(PMe_3)$_2$] (**1a**) possesses two $\tilde{\nu}_{ReH}$ stretching vibrational modes which are separated by *ca.* 30 cm^{-1} in the *Raman* spectrum. These two modes couple with the

$\tilde{\nu}_{XO}$ stretching mode (X = N, C) of the ligand in *trans* position, but do not couple with each other. The coupling leads to significant differences in the IR intensities, so that only the $\tilde{\nu}_{ReH}$ band of the H-ligand *trans* to nitrosyl can be observed in the IR spectrum. These conclusions are based on an analysis of the IR and *Raman* spectra of **1a**, in combination with a theoretical examination of the contributions to the potential-energy distribution in the vibrational modes. Measurements and calculations of the deuterated derivatives **1b** and **1c** provide further evidence for the assignments. The two density-function schemes employed in this work both do reasonably well in predicting molecular geometries and vibrational frequencies. Due to the absence of mode coupling, the intrinsic nitrosyl effects are best seen in $[Re(CO)D_2(NO)(PMe_3)_2]$ (**1c**) where $\tilde{\nu}_{ReD}{}^{t\text{-}NO}$ is calculated to appear *ca.* 45 cm^{-1} below $\tilde{\nu}_{ReD}{}^{t\text{-}CO}$.

Financial support from the *Swiss National Science Foundation* is gratefully acknowledged. We are thankful to Dr. *W. D. Allen*, who provided us with a copy of his INTDER95 program.

REFERENCES

[1] H. Berke, P. Burger, *Comments Inorg. Chem.* **1994**, *16*, 279.
[2] H.-U. Hund, U. Ruppli, H. Berke, *Helv. Chim. Acta* **1993**, *76*, 963; H.-U. Hund, Ph. D. Thesis, Universität Zürich, 1991.
[3] S. Feracin, T. Bürgi, V. I. Bakhmutov, I. Eremenko, E. V. Vorontsov, A. B. Vimenits, H. Berke, *Organometallics* **1994**, *13*, 4194; V. I. Bakhmutov, T. Bürgi, P. Burger, U. Ruppli, H. Berke *ibid.* **1994**, *13*, 4203.
[4] R. H. Crabtree, P. E. M. Siegbahn, O. Eisenstein, A. Rheingold, T. F. Koetzle, *Acc. Chem. Res.* **1996**, *29*, 348; R. H. Crabtree, *J. Organomet. Chem.* **1998**, *557*, 111; R. H. Crabtree, O. Eisenstein, G. Sini, E. Peris, *ibid.* **1998**, *567*, 7.
[5] a) N. V. Belkova, E. S. Shubina, A. V. Ionidis, L. M. Epstein, H. Jacobsen, A. Messmer, H. Berke, *Inorg. Chem.* **1997**, *36,* 1522; b) A. Messmer, H. Jacobsen, H. Berke, submitted.
[6] V. Jonas, W. Thiel, *J. Chem. Phys.* **1995**, *102*, 8474.
[7] V. Jonas, W. Thiel, *J. Chem. Phys.* **1996**, *105*, 3636.
[8] M. J. Frisch, G. W. Trucks, H. B. Schlegel, P. M. W. Gill, B. G. Johnson, M. A. Robb, J. R. Cheeseman, T. Keith, G. A. Petersson, J. A. Montgomery, K. Raghavachari, M. A. Al-Laham, V. G. Zakrzewski, J. V. Ortiz, J. B. Foresman, J. Cioslowski, B. B. Stefanov, A. Nanayakkara, M. Challacombe, C. Y. Peng, P. Y. Ayala, W. Chen, M. W. Wong, J. L. Andres, E. S. Replogle, R. Gomperts, R. L. Martin, D. J. Fox, S. J. Binkley, D. J. Defrees, J. Baker, J. P. Stewart, M. Head-Gordon, C. Gonzalez, J. A. Pople, 'Gaussian 94, Revision D.4', Gaussian, Inc., Pittsburgh PA, 1995.
[9] a) E. J. Baerends, D. E. Ellis, P. E. Ros, *Chem. Phys.* **1973**, *2*, 41; b) G. te Velde, E. J. Baerends, *J. Comp. Phys.* **1992**, *99*, 84; c) C. Fonseca Guera, O. Visser, J. G. Snijders, G. te Velde, E. J. Baerends in 'Methods and Techniques in Computational Chemistry: METECC-95', Ed. E. Clementi and G. Corongiu, STEF, Cagliari, 1995, p. 305; d) G. te Velde, 'ADF 2.1 User's Guide'. Vrije Universiteit, Amsterdam, 1996.
[10] A. D. Becke, *Phys. Rev. A* **1988**, *38*, 3098.
[11] J. P. Perdew, *Phys. Rev. B* **1986**, *33*, 8822; *ibid.* **1986**, *34*, 7046.
[12] D. Andrae, U. Häussermann, M. Dolg, H. Stoll, H. Preuss, *Theor. Chim. Acta* **1990**, *77*, 123.
[13] W. J. Hehre, R. Ditchfield, J. A. Pople, *J. Chem. Phys.* **1971**, *54*, 724; W. J. Hehre, R. Ditchfield, J. A. Pople, *ibid.* **1972**, *56*, 2257; P. C. Hariharan, J. A. Pople, *Theor. Chim. Acta* **1973**, *28*, 213; M. M. Francl, W. J. Pietro, W. J. Hehre, J. S. Binkley, M. S. Gordon, D. J. Defrees, J. A. Pople *J. Chem. Phys.* **1982**, *77*, 3654.
[14] T. H. Dunning, *J. Chem. Phys.* **1971**, *55*, 716.
[15] A. D. McLean, G. S. Chandler, *J. Chem. Phys.* **1980**, *72*, 5639.
[16] T. H. Dunning, *J. Chem. Phys.* **1989**, *90*, 1007; D. E. Woon, T. H. Dunning, *ibid.* **1993**, *98*, 1358.
[17] L. Versluis, Z. Ziegler, *J. Chem. Phys.* **1988**, *88*, 322; L. Fan, L. Versluis, T. Ziegler, E. J. Baerends, W. Ravenek, *Int. J. Quantum Chem.* **1988**, *S22*, 173.
[18] T. Ziegler, V. Tschinke, E. J. Baerends, J. G. Snijders, W. Ravenek, *J. Phys. Chem.* **1989**, *93*, 3050; G. Schreckenbach, J. Li, T. Ziegler, *Int. J. Quantum Chem.* **1995**, *56*, 477.
[19] C. A. Tollman, *Chem. Rev.* **1977**, *77*, 313.
[20] T. Polzer, A. Ellebracht, W. Kiefer, U. Wecker, H. Werner, *J. Organomet. Chem.* **1992**, *438*, 319; T. Polzer, W. Kiefer, *ibid.* **1994**, *472*, 303.

Received December 14, 1998